Magnetic Damping in Polycrystalline Thin-Film math xmlns="http://www.w3.org/1998/Math/MathML" display="inline" overflow="scroll">mi>Fe/mi> mtext>−/mtext>mrow>mrow>mi mathvariant="normal">V/mi>/mrow>/mrow>/math> Alloys

Monika Arora, Erna K. Delczeg-Czirjak, Grant Riley, T.J. Silva, Hans T. Nembach, Olle Eriksson, and Justin M. Shaw

Phys. Rev. Applied **15**, 054031 — Published 14 May 2021

DOI: 10.1103/PhysRevApplied.15.054031

Magnetic damping in polycrystalline Fe-V thin film alloys

Monika Arora[1], Erna K. Delczeg-Czirjak[2], Grant Riley[1,3], T.J. Silva[1], Hans T. Nembach[1,4], Olle Eriksson[2,5], Justin M Shaw[1*]

[1]*Quantum Electromagnetics Division, National Institute of Standards and Technology, Boulder, CO 80305 USA*

[2]*Department of Physics and Astronomy, University Uppsala, S-75120 Uppsala, Sweden*

[3]*Center for Memory and Recording Research, University of California-San Diego, La Jolla, CA 92093 USA*

[4]*JILA, University of Colorado, Boulder, Colorado 80309, USA*

[5]*School of Science and Technology, Örebro University, SE-701 82 Örebro, Sweden*

* corresponding author: justin.shaw@nist.gov

ABSTRACT

We report on the magnetic damping properties of polycrystalline Fe-V alloy thin films that were deposited at room temperature. By varying the concentration of V in the alloy, the saturation magnetization can be adjusted from that of Fe to near zero. We show that an exceptionally low values of the damping parameter can be maintained over the majority of this range with a minimum of the damping at approximately 15-20 % V concentration. Such a minimum is qualitatively reproduced with *ab initio* calculations of the damping parameter although at a concentration closer to 10 % V. The measured intrinsic damping has a minimum value of $(1.53 \pm 0.08) \times 10^{-3}$ which is approximately a factor of 3 higher than our calculated value of 0.48×10^{-3}. From first principles theory, we outline the factors that are mainly responsible for the trend of the damping parameter in these alloys. In particular, the band structure and resulting damping mechanism is shown to change at V concentrations greater than approximately 35 % V content.

INTRODUCTION

Damping of magnetization dynamics has become an important topic for applications in magnetic memories, data storage, magnonics and spin-logic. [1–8] The strength of the damping has a large impact on the speed and energy required to switch or operate such devices. Ideally, the damping parameter would be a parameter that could be independently optimized for a particular application. However, the intrinsic damping can be challenging to engineer since it is largely driven by the details of the bandstructure. [9–17] In particular, it has been shown that the density of states at the Fermi energy $n(E_F)$ is a dominant factor in determining the damping of a metal or half-metal, where a proportionality between damping and $n(E_F)$ was found. [18–23] However, modifying a material's bandstructure through, for example, strain engineering, crystalline phase or alloying the material with other elements may result in undesirable effects on other magnetic properties such as saturation magnetization and magnetic anisotropy. Complicating matters, many extrinsic factors also contribute to the damping such as spin-pumping, eddy currents, radiative damping, and two magnon scattering. [24–33]

For many applications, an extremely low value of the damping parameter α is desired. [4–8] While this can routinely be achieved in insulating materials such as magnetic garnets and ferrites [34–43], this is more challenging in conductors due to the presence of conduction electrons which leads to significant magnon-electron scattering contributions to the damping. [44,45] It was recently shown that Co-Fe alloys can exhibit exceptionally low values of the damping parameter at certain concentrations

due to a sharp minimum in $n(E_F)$. [18] However, this material has an exceptionally high value of the saturation magnetization $\mu_0 M_s$, which can be as high as 2.4 T. Such high values of $\mu_0 M_s$ can be useful for many applications in magnonics since the high $\mu_0 M_s$ yields high magnon velocities and better coupling for transduction. [46] However, for other applications, a material with such a high value of $\mu_0 M_s$ is prohibitive. For example, the critical current for a spin transfer torque magnetic random-access memory cell is proportional to both $\mu_0 M_s$ and α. [47] Thus, any benefit gained from a reduced α may be offset by the higher $\mu_0 M_s$.

As a consequence, it is often desired to have materials that exhibit exceptionally low magnetic damping while simultaneously having low values of $\mu_0 M_s$. Many half-metallic systems can fulfill this requirement, but fabrication requires high temperatures and/or epitaxial growth. [12,13,17,21–23,48–51] One solution may reside in metallic alloys based on Fe and V. Initial calculations by Mankovsky et al., indeed show calculated damping values below 0.001. [52] In addition, since elemental V is not ferromagnetic and the Fe-V alloys adhere to the Slater-Pauling behavior, $\mu_0 M_s$ can be continuously adjusted from that of pure Fe ($\mu_0 M_s$ = 2.1 T) to a value that vanishes ($\mu_0 M_s$ = 0) near 67 % V. Previous work has shown low values of damping in this system, but do not reach the low values predicted by theory. [53–56] More recently, a minimum in the damping parameter approaching 0.001 was found at a composition of ~ 25% V. [57] However, these studies were mostly limited to single crystalline, epitaxial films. For most applications, epitaxial growth is not possible, either due to lack of a single crystalline template (back end processing), thermal budget considerations, and/or throughput considerations. While distinction between single crystal and polycrystalline systems initially appears to be a formality, the additional disorder found in the polycrystalline case can affect the spin scattering rates. This has the potential to have significant impact on the damping parameter, either increasing it or decreasing it depending on the dominate scattering mechanism of the system. [10,14,58,59]

In this work, we address the question about whether the low damping properties can be maintained or possibly improved in room-temperature deposited polycrystalline films suitable for CMOS integration. We compare our results to *ab initio* calculations of the damping parameter. Furthermore, we confirm that the density of states at the Fermi energy largely drives the damping properties in this system. However, due to significant band broadening, this proportionality is not strictly maintained over all compositions.

EXPERIMENT

$Fe_{(1-x)}V_x$ alloys were deposited by co-sputtering from a pure Fe and pure V target with an Ar plasma at a pressure of approximately 0.6 Pa (0.5 mTorr). Rates were calibrated and periodically monitored using x-ray reflectometry. We estimate an upper bound on the uncertainty of the deposition rates to be 5 %. The base pressure of the deposition chamber was approximately 1×10^{-7} Pa (1×10^{-9} Torr). For the majority of samples, the $Fe_{(1-x)}V_x$ layer thickness was fixed at 10 nm. However, for a select subset of alloy concentrations, we deposited a thickness series in order to isolate interfacial properties. To promote good growth and protection from oxidation, a 3 Ta / 5 Cu seed layer and 5 Cu / 3 Ta capping layer was used. X-ray diffraction (XRD) (not shown) reveals a strong [110] texture with a body centered cubic (bcc) crystalline structure, although we will address the possibility of the presence of a more ordered B2 structure later.

Magnetometry was performed by use of a commercial superconducting quantum interference device (SQUID) magnetometer. Here, samples were precisely diced into 6 mm x 6 mm pieces to enable

accurate knowledge of the volume of the $Fe_{(1-x)}V_x$ layer and therefore determination of the saturation magnetization M_s.

Broadband ferromagnetic resonance spectroscopy was performed on samples that were also diced into 6 mm x 6 mm in size. Sample were spin coated with poly methyl methacrylate (PMMA) to prevent electrical shorting before being placed face down on a co-planar waveguide with a center conductor of 100 µm. We used a superconducting magnet to apply magnetic fields of up to $\mu_0 H$ = 3 T perpendicular to the sample surface. As the magnetic field was swept through the FMR condition, the transmission S21 through the CPW was measured by use of a vector network analyzer capable of applying microwaves with a frequency range of 1 – 70 GHz. An example of the measured real and imaginary S21 parameter is given in the inset of Fig. 1 for a 20 % V sample measured at 30 GHz. These spectra are fit to the dynamic susceptibility as outlines in Ref [[60]] to determine the resonance field H_{res} and linewidth ΔH for a given frequency f. As this data is acquired over a large range of frequency, we generate plots of the H_{res} and ΔH as functions of f, examples of which are shown in Figs. 1(a) and 1(b), respectively. Also included in Fig. 1(a) are the fits to the following equation that is used to determine the perpendicular anisotropy and spectroscopic g-factor.

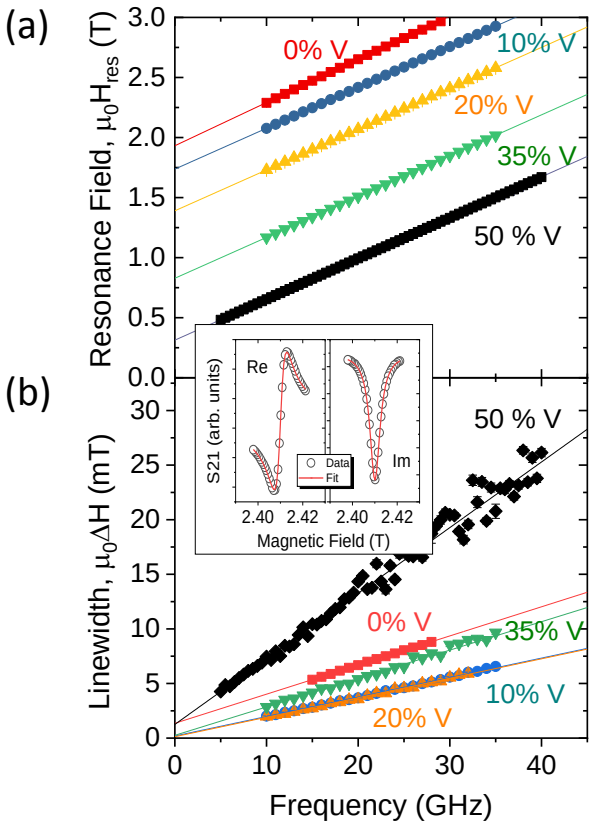

Figure 1. (a) Resonance field and (b) linewidth versus frequency for several compositions of 10 nm thick FeV films. The inset is an example of the VNA-FMR spectrum and fits of the susceptibility to the data for the 20 % V sample at 30 GHz.

$$f = \frac{\mu_0 \mu_B g}{2\pi\hbar}\left(H_{res} - M_{eff}\right) \tag{1}$$

where g is the spectroscopic g-factor, μ_0 is the permeability of free space, μ_B is the Bohr magneton, and $\hbar$ is the reduced Planck's constant. The effective magnetization M_{eff} is defined as $M_{eff} = M_s - H_k$, where H_k is the perpendicular anisotropy field. Similarly, the magnetic damping parameter α and inhomogeneous contribution to the linewidth ΔH_0 are determined by fits of the following equation to the frequency dependence of the linewidth ΔH,

$$\Delta H = \Delta H_0 + \frac{4\pi\alpha}{\gamma\mu_0} f \quad (2)$$

where $\gamma = (\mu_B g)/\hbar$. The perpendicular geometry was intentionally chosen to minimize contributions to the linewidth from 2-magnon scattering. [27–32] In addition, all samples greater than 5 nm in thickness were measured using a 60 μm thick sapphire spacer placed between the sample and the waveguide to minimize any radiative damping contributions. [33] Calculations of the radiative damping contribution indicate that it is negligible within these measurement conditions.

DETAILS OF THE CALCULATION

The electronic structure is obtained solving the Kohn-Sham equations as implemented in the spin-polarized relativistic Korringa-Kohn-Rostoker (SPR-KKR) code. [61] The chemical disorder was treated within the coherent potential approximation (CPA). [62,63] The Perdew-Burke-Ernzerhof [64] exchange-correlation functional was employed. Bandstructures represented by the Bloch spectral functions (BSF) are calculated within the scalar relativistic approximation as presented by Ebert *et al.* [65]

To obtain the damping parameter, the Dirac equation was solved within the atomic sphere approximation. The angular momentum cutoff of l_{max}= 4 was used in the multiple scattering expansion. A *k*-point grid consisting of ≈1600 points in the irreducible Brillouin zone was employed for the self-consistent calculations, and more than 1,500,000 for the damping calculations. The damping parameter, α, evaluated at 300 K was calculated via the linear response theory. [9] An alloy analogy model within CPA was considered in order to include the temperature effects in the scattering process of electrons with respect to atomic displacement. [66] The ”scattering-in” term of the Boltzmann equations was taken into account via vertex corrections. [67] All calculations are done for the experimental lattice parameters obtained from the Pearson crystal database, [68] that are specifically: 0.2856 nm for Fe [69], 0.2878 nm for $Fe_{0.9}V_{0.1}$ [70], 0.2892 nm for $Fe_{0.8}V_{0.2}$ [71], 0.2900 nm for $Fe_{0.7}V_{0.3}$ [72], 0.2905 nm for $Fe_{0.65}V_{0.35}$ [73], 0.2911 nm for $Fe_{0.55}V_{0.45}$ [74], 0.2916 nm for $Fe_{0.5}V_{0.5}$ [75] bcc alloys and 0.291 nm for FeV in the B2 (CsCl) structure. [75] Value for $Fe_{0.6}V_{0.4}$ is interpolated from the $Fe_{0.55}V_{0.45}$ and $Fe_{0.65}V_{0.35}$ data. Debye temperature (T_D) of FeV alloys for the damping calculations are extrapolated from the Fe and V room temperature experimental values. [76] It is important to point out that these lattice constants are room temperature values, which will partially take some of the thermal effects (i.e., thermal expansion) into account. As a check, the lattice constant for the $Fe_{50}V_{50}$ sample was verified to be within 1 % of the tabulated bulk values. Such a variation of the lattice constant will cause a change in the calculated damping constant of less than 10 %. As we will later see, this is outside of any meaningful range.

RESULTS

Figure 2 shows that the saturation magnetization $\mu_0 M_s$ and effective magnetization $\mu_0 M_{eff}$ decrease in an almost linear fashion as the V content increases, which is consistent with previous reports. [54,56,57,77] This is expected from the simplified band-filling Slater-Pauling model. This model predicts that the magnetization should vanish at a concentration of 67 % V. Indeed, even more thorough calculations of magnetic moment show little deviation from these simpler models. [77] Projecting our data to higher V concentrations shows that the magnetization will vanish at approximately 60 % V. This small deviation could be a result of the limitation of the Slater-Pauling model, finite temperature effects,

errors in the deposition rates/stoichiometry, and/or interfacial effects. However, two previous reports also show a vanishing value of $\mu_0 M_s$ at 60 % V. [54,77] From an applications standpoint, the data in Fig. 2 is desired since it shows the straightforward ability to tune both $\mu_0 M_s$ and $\mu_0 M_{eff}$ over a large range of values.

Unlike the trends in M_s, Fig. 3(a) shows that the g-factor exhibits little variation as a function of composition – exhibiting only a small increase from $g \approx 2.08$ to $g \approx 2.10$ from pure Fe to 10 % V, which is consistent with what was found in epitaxial films. [57] However, our data also exhibits significant scatter. The scatter was reduced by use of the asymptotic analysis to the determination of the g-factor. [78] However, given the high value of saturation magnetization and limited magnetic field, we were unable to apply this method to the pure Fe sample. We include a value of the g-factor for pure Fe taken from Schoen *et al*. to provide an additional data point. [79] Even with the scatter of the data, these results show that the orbital moment and therefore the spin-orbit interaction do not vary significantly as a function of concentration. This is not surprising given the fact that Fe and V have similar atomic numbers at 26 and 23, respectively.

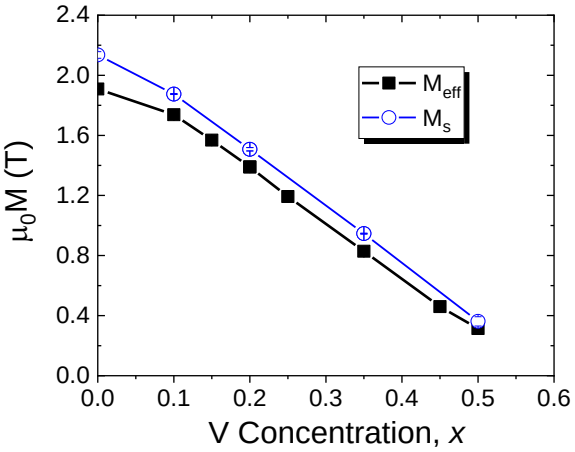

Figure 2. Saturation magnetization and effective magnetization versus the V concentration.

The damping parameter for the 10 nm thick layers as a function of V concentration are shown as the black data points in Fig. 3(b). The data show a minimum value in the vicinity of 15 % V. However, even at a thickness of 10 nm, there will be a significant spin-pumping contribution to the damping. [24,80,25,81] To quantitatively account for spin-pumping effects, we measured the damping as a function of thickness for samples with V concentration of 0%, 10 %, 20 %, 35 %, and 50 %. Figure 3(c) shows an example of damping versus the inverse thickness for 20 % V. As expected from spin-pumping theory, the data exhibits a linear behavior versus inverse thickness. The *y*-intercept corresponds to the value of the damping parameter with the spin-pumping contribution removed, whereas the slope is equal to $(g\mu_B g^{\uparrow\downarrow}_{eff})/(4\pi M_s)$ where $g^{\uparrow\downarrow}_{eff}$ is the effective real part of the spin-mixing conductance. Since there are no other known contributions to the damping, these values obtained from the y-intercepts are identified as the intrinsic damping of the material and is plotted in Fig. 3(b) as the blue data. These data also show a minimum value, but it is shifted to a higher V concentration of approximately 20 % V relative to the uncorrected data for the 10 nm samples. This trend can be understood from the fact that the spin-pumping contribution is proportional to $1 / M_s$. Combined with the variation of $g^{\uparrow\downarrow}_{eff}$ as a function of concentration, the spin-pumping contribution should increase substantially with the increased V concentration. This is explicitly shown in Fig. 3(d) where both $g^{\uparrow\downarrow}_{eff}$ and the ratio of $g^{\uparrow\downarrow}_{eff} / \mu_0 M_s$ are plotted. The latter quantity indicates how the spin-pumping contribution will vary with composition since it is proportional to that contribution for a given thickness.

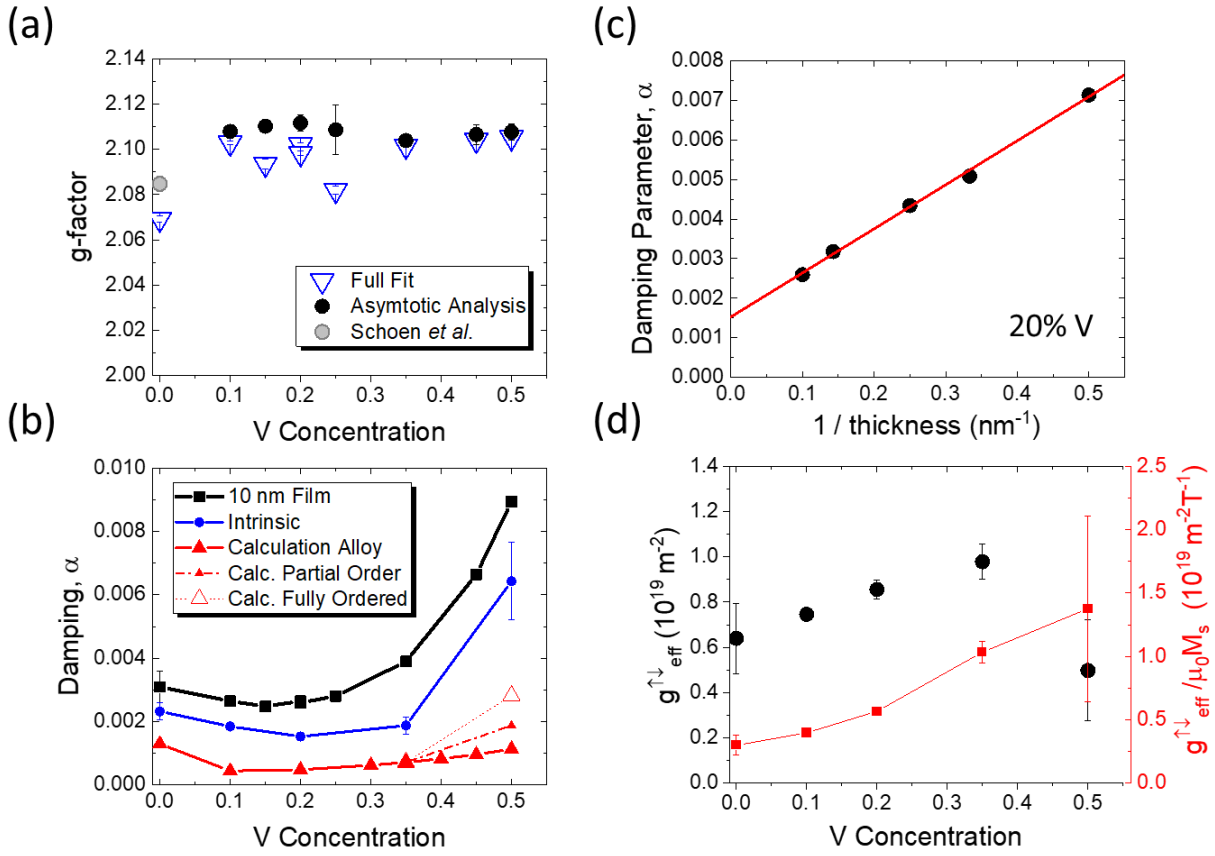

Figure 3. (a) Spectroscopic g-factor versus V concentration for the 10 nm thick films. Gray data point is taken from Ref. [[79]], (b) Damping parameter for the 10 nm films (black square), intrinsic values (blue circle) and *ab-initio* calculated values (red triangles) versus the V concentration. The open triangle represent calculations with increased amounts of B2 order. (c) An example of the dependence of the damping parameter on inverse thickness used to account for the spin-pumping contribution for the 20 % V samples. The red line is a linear fit through the data. (d) Plot of the effective spin-mixing conductance and effective spin-mixing conductance divided by the saturation magnetization versus the V concentration of the alloy.

AB INITIO CALCULATIONS

Also included in Fig. 3(b) are the *ab-initio* calculated values of the damping parameter (red filled triangles). These values should be compared to the intrinsic contribution to the damping (blue curve in Fig.3b) and two distinct features stand out in this comparison. First of all, we note that for lower V concentrations (up to 35 %) the trend of the calculated damping parameter is consistent with the observed values, albeit with an approximately factor of two or more reduced value. Secondly, for higher V concentrations (larger than 35 %) the trend in the experimental data, which shows a sharp increase in the damping with higher V concentration, is not at all captured by theory. We will return to the latter aspect below, but note first that the damping parameters presented here are in good agreement with those shown in Ref. [[52]] calculated for 300 K. Secondly, we note that the reproduction of extremely

low values of the damping parameter, as is the case in this investigation, is notoriously difficult for ab-initio theory. [15,52]

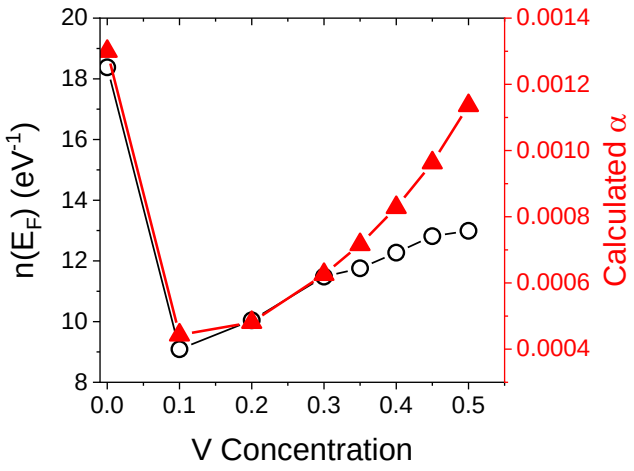

Figure 4. Calculated density of states at the Fermi energy $n(E_F)$ (left y-axis, black open circles) in comparison with the theoretical damping parameter (right y-axis, red filled triangles) as a function of V

In order to further analyze the trend in the calculated damping parameter we compare the calculated damping parameter (red filled triangles) with the density of states at the Fermi level, $n(E_F)$ (black open circles) in Fig. 4. Hence, Fig. 4 compares two sets of theoretical data. It can be seen that the damping parameter follows that of the $n(E_F)$ up to approximately 35 % V, where the damping is seen to increase more rapidly relative to the DOS at the Fermi energy. A microscopic explanation to this behavior can be found from a detailed analysis of the electronic structure, as represented by the Bloch spectral functions (BSFs) in Fig. 5. For lower V concentrations the energy bands (as represented by the BSF) are relatively well defined, without any major change between alloys with different V concentrations. However, at approximately 35 % V there is a distinct change in the BSF. This is illustrated in Fig. 5., where we show BSFs for spin-up and spin down states, for 30 % (upper panels) and 50 % (lower panels) V concentrations. First it should be noted that for the spin-down states, the energy dispersion has very sharp, band like features, that are similar for both alloy concentrations. This is due to the similar scattering properties of spin-down Fe and V states in the bcc structure. Note that for the spin-down states the BSFs are particularly sharp for states around the Fermi energy [$E_F = E(k) = 0$], which allows to identify sharp features of the Fermi surface for these states.

In contrast, the situation is drastically different for the spin-up states. Figure 5 shows that most features in the spin-up state are considerably more smeared out or broadened compared to spin-down states, a consequence of the difference in scattering properties of spin up Fe and V in the bcc structure. This is caused by the fact that the spin-down potential of Fe atoms places the 3d states at similar energy as that of 3d states of V, meaning that spin-down 3d electrons experience an almost perfect lattice without disorder. The exchange splitting of Fe causes the spin-up 3d states to lie considerably below the spin-up states of V, which causes significantly different scattering properties. The CPA method therefore results in more smeared electron states for the spin-up states.

It is also shown that for lower V concentrations, the energy dispersion is reasonably well described in terms of energy bands, with a well-defined dispersion (exemplified by the green shaded bands at and below E_F). However, for higher V concentrations (e.g. at 50 %) a clear band dispersion is lacking, at least for some regions of the Brillouin zone. An example of this behavior is noticeable from the energy states along the Γ-H, Γ-N and Γ-P directions, where the 3d electronic states dominate. This is again most noticeable in the green shaded regions at and below E_F becoming much more smeared out

relative to the 30 % V sample indicating that a quasi-particle description of the spin state is no longer possible. As a consequence, the electronic channels that allow for energy dissipation become drastically modified at around 35 % V concentration. It is therefore expected that at around 35 %, the calculated damping and the n(E_F) should not have the same trend as function of V concentration as the data in Fig. 4 explicitly shows.

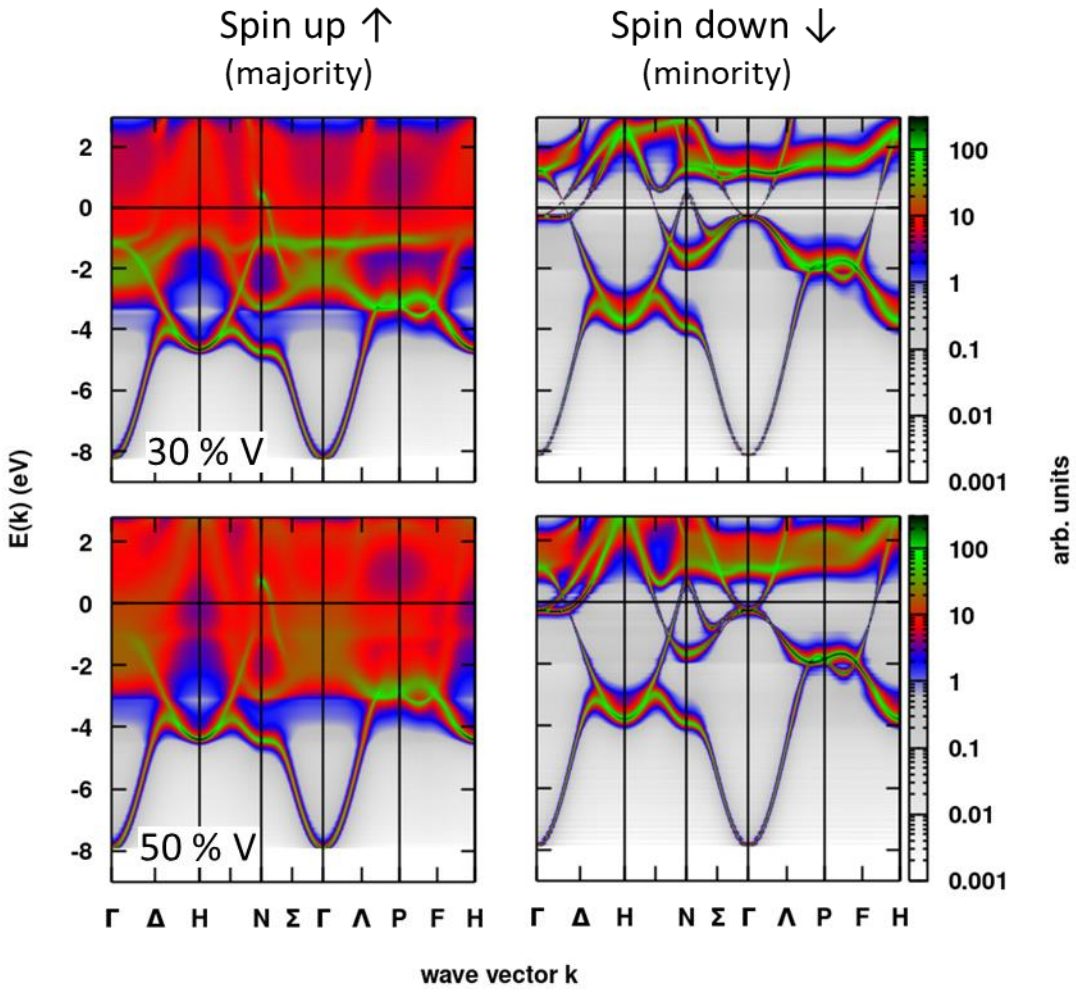

Figure 5 Spin-polarized Bloch spectral function (BSF) for 30 % V (upper panels) and 50 % V (lower panels) alloys. The color scale is in arbitrary units.

Even with these considerations in mind, the experimental data shows a much more pronounced enhancement of the damping parameter at V concentrations above 35 % V [see Fig. 3(b)], something which may reflect a shortcoming of the CPA description of the electronic structure and damping of this system. In other words, the calculated increase in damping due to the non-quasi-particle behavior of the electron states of the spin-up channel are not adequate enough to describe the much more pronounced increase in the damping found in the experimental data. An alternative explanation for the experimental trend may reside in consideration of the presence of higher crystalline order within the FeV alloy. Indeed, at concentration of 50 % V, the Fe-V system can adopt a fully ordered B2 phase (CsCl structure) where Fe and V occupy different interpenetrating sublattices offset by (a/2, a/2, a/2) where a

is the simple cubic lattice constant. We refer to this as the fully ordered $Fe_{50}V_{50}$ intermetallic phase. There are naturally intermediate scenarios between these two extremes, which typically is referred to as partial ordering where each sublattice can have a preferential occupation of Fe or V that is in between the completely disordered alloy and the fully ordered intermetallic phase. For the example that we present here, we focus on a partially ordered state where one sublattice has an 80 % preferential occupancy of Fe (i.e., $Fe_{80}V_{20}$) and the other sublattice has an 80 % preferential occupancy of V (i.e., $Fe_{20}V_{80}$).

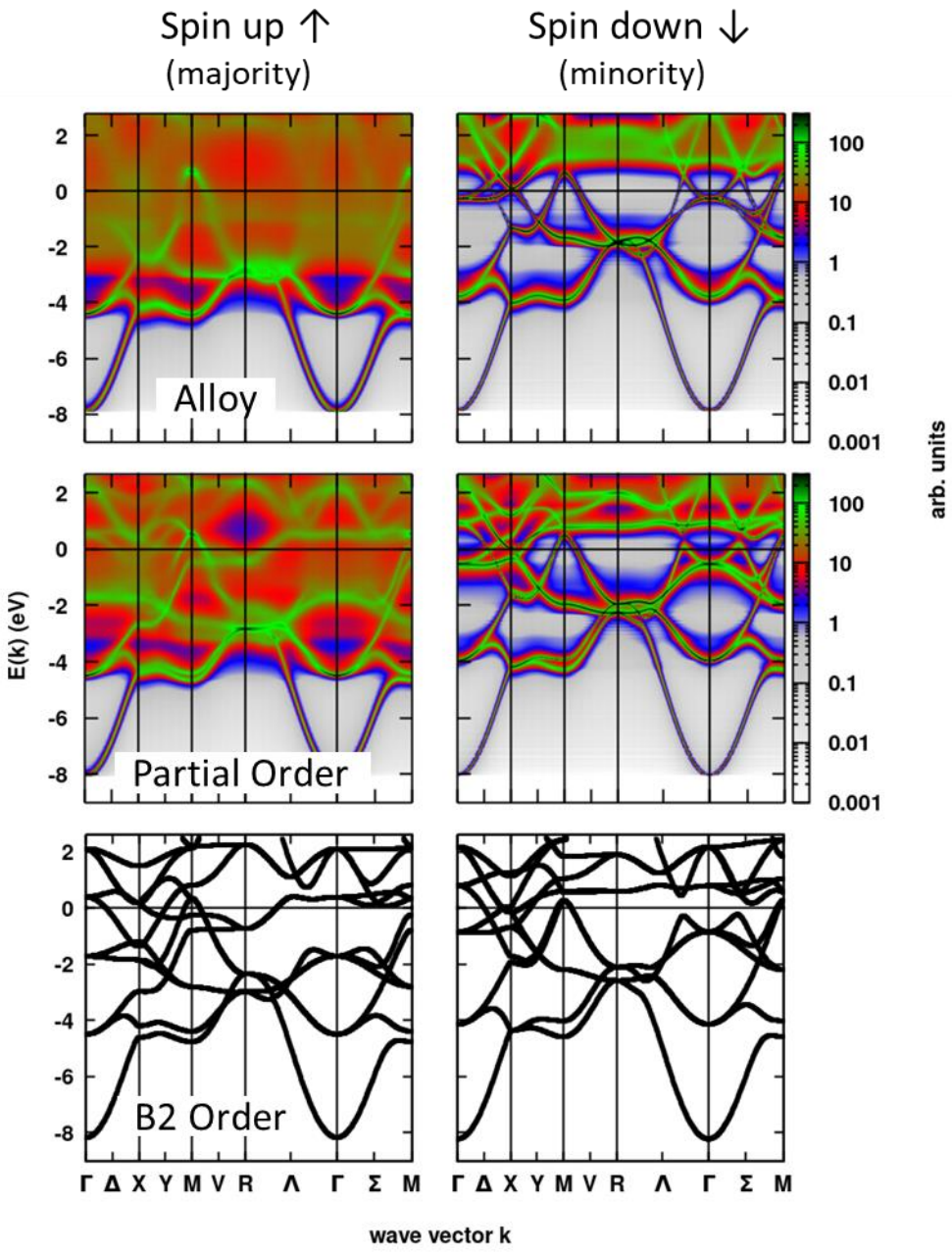

Figure 6. Spin-polarized Bloch spectral function (BSF) for 50 % V in B2 structure. Alloy (upper panels) represents random distribution of Fe and V in the two sublattices, partial ordering (middle panels)

outline an 80 % preferential occupancy of Fe in one sublattice and the other sublattice has an 80 % preferential occupancy of V. In the fully ordered B2 structure (lower panels), Fe and V occupy separate sublattices. The color scale is in arbitrary units.

The calculated damping constants for the fully ordered and partially ordered phases are included in Fig. 3(b). It is immediately apparent that the partial and full order, respectively, increase the calculated damping constant by a factor of ~ 0.6 and ~ 1.5 relative to the disordered alloy, and shows better agreement with the trends in the experimental data. However, XRD did not reveal the additional (001) and (111) reflections that would be expected to appear with B2 order in these samples. However, the scattering factors for Fe and V are very similar owing to their similar atomic numbers. [82] As a result, simulations show the relative intensity of these peaks to that of the (011) peak to be 0.9% and 0.3% respectively. This combined with small signal that results from the polycrystalline structure and broad linewidths renders the (001) and (111) peaks virtually undetectable for our samples with a standard laboratory based x-ray source. As a result, no conclusions can be made about the presence or absence of any B2 order in our samples. The use of resonant XRD at facility based light sources to search for order in this system would be desired in the future.

The microscopic explanation for the increased damping causing by increased ordering is demonstrated via the BSF, plotted for Fe-V alloys with various degrees of order plotted in Fig. 6. Here, it is seen that the partial ordering of Fe and V atoms will influence the electronic structure, and in particular, the width of the BSFs. Comparing the disordered alloys (top panels) and partially ordered alloys (middle panels) bandstructures reveals that ordering sharpens the band features, in particular for the spin up states (the spin down states are sharp for all degrees of partial ordering). The most dramatic effects are found along high symmetry directions of the Brillouin zone, like Γ–R, Γ–M and Γ–X. In the case of full ordering (bottom panels), the BSF is represented by sharp and well-defined bands.

The width of the BSFs greatly influences the damping. Calculations of the damping parameter are often made as a function of this width, and a general trend is that the damping initially decreases with the BSF width, in the regime of intraband scattering, to reach a minimum, whereupon for larger widths, in the regime of inter band scattering, the damping increases again. [83] However, the band broadening comes mainly from the chemical disorder in the present calculations, the trend of the BSFs shown in Fig. 6 can ~~therefore~~ explain, to some extent, why the calculated damping increases with increased order; it is a consequence of the BSFs that become narrower for larger degrees of ordering of Fe and V on the two sublattices. Furthermore, based on these considerations, we offer an explanation of the experimental data shown in Fig.3(b), and in particular, the sharp increase of the damping parameter above 35 % V. A partial ordering of Fe and V on the two sublattices, that sets in for V concentrations higher than 35 %, would again be consistent with the measured damping parameters.

As a final point, we remark that above we analyzed the electronic structure by means of the BSFs calculated at 0 K. Since Gilbert damping parameters are calculated at finite temperature, for a complete analysis, temperature dependent BSFs would be required, that is not available at present. Here, we fully capture changes in the band structure at the Fermi energy as well as for bands below and above it due to composition variation and ordering. The close lying bands around E_F may be repopulated at elevated temperatures, therefore, changes in the sharpness of the bands below and above E_F due to V doping and ordering are relevant to discuss. An inspection of the Fermi surface alone, done for instance recently in a work by Sipr *et al*. [84], could miss important changes in bands below and above E_F. Finally, our BSF analysis is in line with the above described model presented in Ref. 84, however the additional

band broadening due to the finite temperature is not included. As a consequence, the intra- and interband scattering contribution cannot be quantified either.

DISCUSSION

For technological applications, a low intrinsic damping may not be sufficient since the total damping ultimately determines device performance. Thus, it is important to consider the total linewidth that includes extrinsic contributions. A potential dominant contribution to the total linewidth is the inhomogeneous linewidth $\mu_0\Delta H_0$. Inhomogeneity in a film can also translate into device-to-device variations when such a film is patterned into nanosized features. [85] Figure 7 is a plot of $\mu_0\Delta H_0$ versus V concentration. All samples have values below 1.5 mT and with the exception of the pure Fe and 50 % V sample, it is at or below 0.6 mT. These data show sputter deposited films can be produced with minimal extrinsic contribution to the linewidth. In fact, these values are almost an order of magnitude lower than those found in similar epitaxial films measured in the same geometry. [57] However, it is not uncommon for epitaxial systems to have a larger $\mu_0\Delta H_0$, especially when measured in the perpendicular geometry. Despite the difference in $\mu_0\Delta H_0$, comparison of the intrinsic damping parameters between polycrystalline FeV studied here and epitaxial $Fe_{(1-x)}V_x$ layers found in Ref. [[57]] show very little difference as displayed in Fig. 8. Any increase of structural disorder from the polycrystalline films causes only a minimal change of the damping parameter relative to the epitaxial data. This suggests that either the damping mechanism is not strictly intraband or interband scattering alone, or that the spin scattering rates are not dominated by the structural disorder of the system.

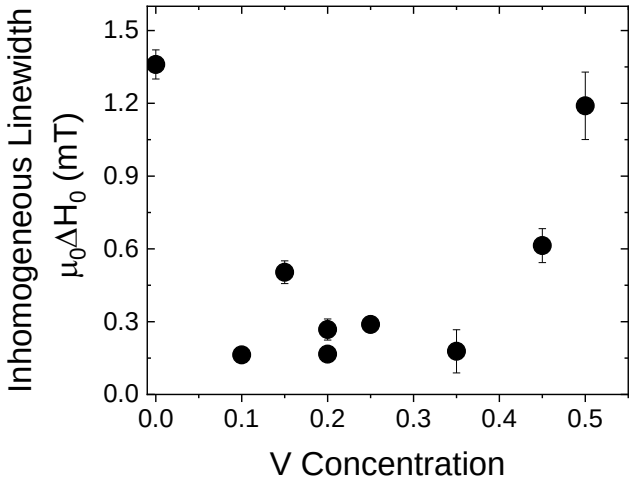

Figure 7. Plot of the inhomogeneous linewidth for the 10 nm thick samples versus V concentration.

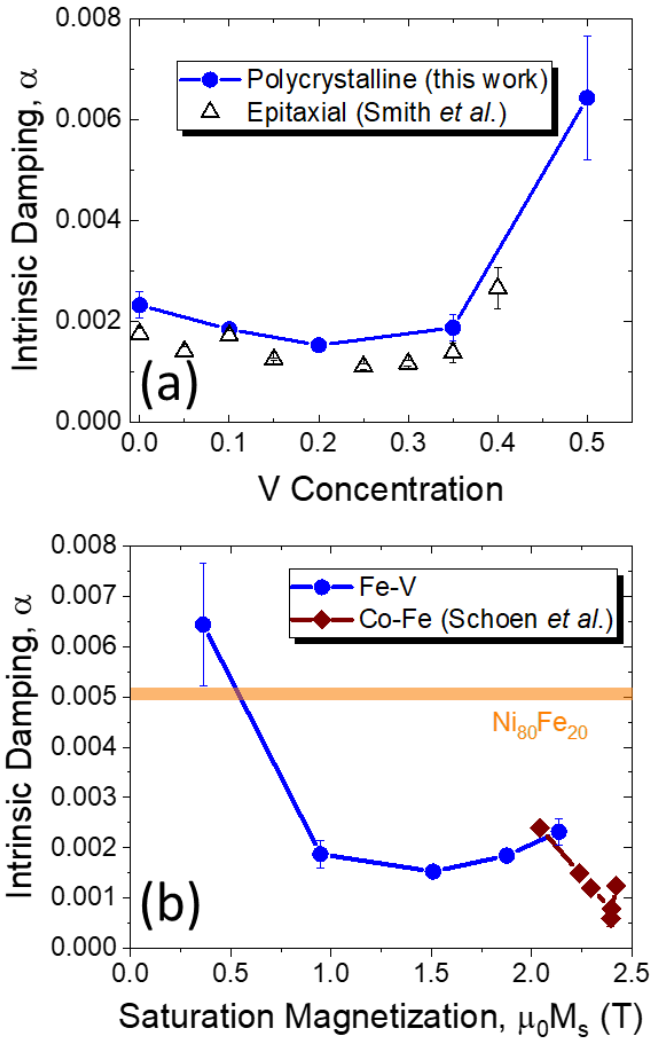

Figure 8. (a) Comparison of the intrinsic damping between epitaxial films reported in Smith *et al*. [57] and polycrystalline films as a function of the V concentration. (b) Intrinsic damping of Co-Fe films taken from Schoen *et al.* [18] and Fe-V films (present work) versus the saturation magnetization. The horizontal line is the intrinsic value for permalloy, $Ni_{80}Fe_{20}$.

In Fig. 8(b), we plot the damping parameter versus $\mu_0 M_s$ for the Fe-V alloys along with the those of similar Co-Fe alloys found in Ref. [[18]] that range in composition from 0 % Co (pure Fe) to 35% Co ($Co_{35}Fe_{65}$). These data demonstrate that exceptionally low values of the damping parameter (< 0.0025) can be maintained over a large range of $\mu_0 M_s$ that spans 2.4 T to approximately 0.8 T. Furthermore, these alloys are produced through room temperature sputtering methods that are compatible with CMOS fabrication. It is especially interesting to compare the 35 % V sample to Permalloy ($Ni_{80}Fe_{20}$), which is one of the most used and studied ferromagnetic metals, especially in the field of spintronics and magnonics. [3] The damping parameter of $Ni_{80}Fe_{20}$ is also indicated in Fig. 8(b). At this concentration, $\mu_0 M_s$ of both materials is approximately 1 T, but the damping parameter of the $Fe_{65}V_{35}$ is

0. 0019—a factor of ≈ 2.5 smaller than permalloy. [86] For applications in magnonics, lower damping is desired since the lifetime of a spin excitation is increased with lower damping. From a damping perspective, this suggests that Fe-V is a suitable replacement for permalloy for some applications. Of course, permalloy also possesses other desirable qualities such as vanishing magnetostriction. However, in the case of FeV, the magnetostriction has a zero crossing at approximately 5-8 % V, but the amplitude of the saturation magnetostriction was found to be relatively low at < 12 ppm over the range of concentrations studied here. [87–89]

SUMMARY

In summary, we have measured the intrinsic damping parameter in polycrystalline, sputter-deposited Fe-V alloys that span the range from pure Fe to 50 % V in atomic concentration. The intrinsic damping shows a minimum value of $(1.53 \pm 0.08) \times 10^{-3}$ at approximately 20 % V. Extremely low values of the damping parameter are found for alloys with a concentration at or below 35 % V. Above this concentration, there is a larger increase in the damping as the V content is increased. In addition, the saturation magnetization is confirmed to continuously vary as predicted from the Slater-Pauling model. *Ab initio* calculations qualitatively reproduce the trends in the damping parameter. However, for the alloys with more than 35 % V, some degree of partial B2 order is needed to describe the increase in the damping found in the experimental data. This increase in damping for higher V content is explained through sharpening of the majority Bloch spectral functions, as more B2 order is introduced.

ACKNOWLEDGEMENTS

G.R. acknowledges support from U.S. Department of Energy award No. DE-SC0018237. O.E. acknowledges support from the Knut och Alice Wallenberg (KAW) foundation, the Swedish research council (VR), the Foundation for Strategic Research (SSF), the Swedish energy agency (Energimyndigheten), eSSENCE, STandUPP, and the ERC (synergy grant). E.K.D-Cz. acknowledges Sergey Mankovsky for technical support.

REFERENCES

[1] S. Mangin, Y. Henry, D. Ravelosona, J. A. Katine, and E. E. Fullerton, *Reducing the Critical Current for Spin-Transfer Switching of Perpendicularly Magnetized Nanomagnets*, Appl. Phys. Lett. **94**, 012502 (2009).

[2] P. B. Visscher and S. Wang, *LLG Simulation of MRAM Switching Trajectories*, IEEE Transactions on Magnetics **42**, 3198 (2006).

[3] V. V. Kruglyak, S. O. Demokritov, and D. Grundler, *Magnonics*, J. Phys. D **43**, 264001 (2010).

[4] A. V. Chumak, V. I. Vasyuchka, A. A. Serga, and B. Hillebrands, *Magnon Spintronics*, Nature Physics **11**, 453 (2015).

[5] B. Lenk, H. Ulrichs, F. Garbs, and M. Münzenberg, *The Building Blocks of Magnonics*, Physics Reports **507**, 107 (2011).

[6] S. Neusser and D. Grundler, *Magnonics: Spin Waves on the Nanoscale*, Advanced Materials **21**, 2927 (2009).

[7] T. Brächer and P. Pirro, *An Analog Magnon Adder for All-Magnonic Neurons*, Journal of Applied Physics **124**, 152119 (2018).

[8] K. Vogt, F. Y. Fradin, J. E. Pearson, T. Sebastian, S. D. Bader, B. Hillebrands, A. Hoffmann, and H. Schultheiss, *Realization of a Spin-Wave Multiplexer*, Nat Commun **5**, 3727 (2014).
[9] H. Ebert, S. Mankovsky, D. Ködderitzsch, and P. J. Kelly, *Ab Initio Calculation of the Gilbert Damping Parameter via the Linear Response Formalism*, Phys. Rev. Lett. **107**, 066603 (2011).
[10] K. Gilmore, Y. U. Idzerda, and M. D. Stiles, *Identification of the Dominant Precession-Damping Mechanism in Fe, Co, and Ni by First-Principles Calculations*, Phys. Rev. Lett. **99**, 027204 (2007).
[11] I. Turek, J. Kudrnovský, and V. Drchal, *Nonlocal Torque Operators in \textit{ab Initio} Theory of the Gilbert Damping in Random Ferromagnetic Alloys*, Phys. Rev. B **92**, 214407 (2015).
[12] J. Chico, S. Keshavarz, Y. Kvashnin, M. Pereiro, I. Di Marco, C. Etz, O. Eriksson, A. Bergman, and L. Bergqvist, *First-Principles Studies of the Gilbert Damping and Exchange Interactions for Half-Metallic Heuslers Alloys*, Phys. Rev. B **93**, 214439 (2016).
[13] C. Liu, C. K. A. Mewes, M. Chshiev, T. Mewes, and W. H. Butler, *Origin of Low Gilbert Damping in Half Metals*, Applied Physics Letters **95**, 022509 (2009).
[14] B. Khodadadi, A. Rai, A. Sapkota, A. Srivastava, B. Nepal, Y. Lim, D. A. Smith, C. Mewes, S. Budhathoki, A. J. Hauser, M. Gao, J.-F. Li, D. D. Viehland, Z. Jiang, J. J. Heremans, P. V. Balachandran, T. Mewes, and S. Emori, *Conductivitylike Gilbert Damping Due to Intraband Scattering in Epitaxial Iron*, Phys. Rev. Lett. **124**, 157201 (2020).
[15] F. S. M. Guimarães, J. R. Suckert, J. Chico, J. Bouaziz, M. dos S. Dias, and S. Lounis, *Comparative Study of Methodologies to Compute the Intrinsic Gilbert Damping: Interrelations, Validity and Physical Consequences*, J. Phys.: Condens. Matter **31**, 255802 (2019).
[16] T. Qu and R. H. Victora, *Dependence of Kambersky Damping on Fermi Level and Spin Orientation*, Journal of Applied Physics **115**, 17C506 (2014).
[17] C. Guillemard, S. Petit-Watelot, L. Pasquier, D. Pierre, J. Ghanbaja, J.-C. Rojas-Sánchez, A. Bataille, J. Rault, P. Le Fèvre, F. Bertran, and S. Andrieu, *Ultralow Magnetic Damping in ${\mathrm{Co}}_{2}\mathrm{Mn}$-Based Heusler Compounds: Promising Materials for Spintronics*, Phys. Rev. Applied **11**, 064009 (2019).
[18] M. A. W. Schoen, D. Thonig, M. L. Schneider, T. J. Silva, H. T. Nembach, O. Eriksson, O. Karis, and J. M. Shaw, *Ultra-Low Magnetic Damping of a Metallic Ferromagnet*, Nat Phys **12**, 839 (2016).
[19] S. Srivastava, A. P. Chen, T. Dutta, R. Ramaswamy, J. Son, M. S. M. Saifullah, K. Yamane, K. Lee, K.-L. Teo, Y. P. Feng, and H. Yang, *Effect of ${({\mathrm{Co}}_{x}{\mathrm{Fe}}_{1\ensuremath{-}x})}_{80}{\mathrm{B}}_{20}$ Composition on the Magnetic Properties of the Free Layer in Double-Barrier Magnetic Tunnel Junctions*, Phys. Rev. Applied **10**, 024031 (2018).
[20] H. Lee, Y.-H. A. Wang, C. K. A. Mewes, W. H. Butler, T. Mewes, S. Maat, B. York, M. J. Carey, and J. R. Childress, *Magnetization Relaxation and Structure of CoFeGe Alloys*, Applied Physics Letters **95**, 082502 (2009).
[21] S. Mizukami, D. Watanabe, M. Oogane, Y. Ando, Y. Miura, M. Shirai, and T. Miyazaki, *Low Damping Constant for Co2FeAl Heusler Alloy Films and Its Correlation with Density of States*, Journal of Applied Physics **105**, 07D306 (2009).
[22] B. Pradines, R. Arras, I. Abdallah, N. Biziere, and L. Calmels, *First-Principles Calculation of the Effects of Partial Alloy Disorder on the Static and Dynamic Magnetic Properties of ${\mathrm{Co}}_{2}\mathrm{MnSi}$*, Phys. Rev. B **95**, 094425 (2017).
[23] J. M. Shaw, E. K. Delczeg-Czirjak, E. R. J. Edwards, Y. Kvashnin, D. Thonig, M. A. W. Schoen, M. Pufall, M. L. Schneider, T. J. Silva, O. Karis, K. P. Rice, O. Eriksson, and H. T. Nembach, *Magnetic Damping in Sputter-Deposited $\mathrm{C}{\mathrm{o}}_{2}\mathrm{MnGe}$ Heusler Compounds with $A2,B2$, and $L{2}_{1}$ Orders: Experiment and Theory*, Phys. Rev. B **97**, 094420 (2018).
[24] Y. Tserkovnyak, A. Brataas, and G. E. W. Bauer, *Enhanced Gilbert Damping in Thin Ferromagnetic Films*, Phys. Rev. Lett. **88**, 117601 (2002).

[25] O. Mosendz, V. Vlaminck, J. E. Pearson, F. Y. Fradin, G. E. W. Bauer, S. D. Bader, and A. Hoffmann, *Detection and Quantification of Inverse Spin Hall Effect from Spin Pumping in Permalloy/Normal Metal Bilayers*, Phys. Rev. B **82**, 214403 (2010).

[26] M. Sparks, R. Loudon, and C. Kittel, *Ferromagnetic Relaxation. I. Theory of the Relaxation of the Uniform Precession and the Degenerate Spectrum in Insulators at Low Temperatures*, Phys. Rev. **122**, 791 (1961).

[27] M. J. Hurben and C. E. Patton, *Theory of Two Magnon Scattering Microwave Relaxation and Ferromagnetic Resonance Linewidth in Magnetic Thin Films*, Journal of Applied Physics **83**, 4344 (1998).

[28] R. D. McMichael, D. J. Twisselmann, J. E. Bonevich, A. P. Chen, W. F. Egelhoff, and S. E. Russek, *Ferromagnetic Resonance Mode Interactions in Periodically Perturbed Films*, Journal of Applied Physics **91**, 8647 (2002).

[29] P. Krivosik, N. Mo, S. Kalarickal, and C. E. Patton, *Hamiltonian Formalism for Two Magnon Scattering Microwave Relaxation: Theory and Applications*, Journal of Applied Physics **101**, 083901 (2007).

[30] R. D. McMichael, *A Mean-Field Model of Extrinsic Line Broadening in Ferromagnetic Resonance*, Journal of Applied Physics **103**, 07B114 (2008).

[31] J. Lindner, K. Lenz, E. Kosubek, K. Baberschke, D. Spoddig, R. Meckenstock, J. Pelzl, Z. Frait, and D. L. Mills, *Non-Gilbert-Type Damping of the Magnetic Relaxation in Ultrathin Ferromagnets: Importance of Magnon-Magnon Scattering*, Phys. Rev. B **68**, 060102 (2003).

[32] I. Barsukov, F. M. Römer, R. Meckenstock, K. Lenz, J. Lindner, S. Hemken to Krax, A. Banholzer, M. Körner, J. Grebing, J. Fassbender, and M. Farle, *Frequency Dependence of Spin Relaxation in Periodic Systems*, Phys. Rev. B **84**, 140410 (2011).

[33] M. A. W. Schoen, J. M. Shaw, H. T. Nembach, M. Weiler, and T. J. Silva, *Radiative Damping in Waveguide-Based Ferromagnetic Resonance Measured via Analysis of Perpendicular Standing Spin Waves in Sputtered Permalloy Films*, Phys. Rev. B **92**, 184417 (2015).

[34] R. Karim, S. D. Ball, J. R. Truedson, and C. E. Patton, *Frequency Dependence of the Ferromagnetic Resonance Linewidth and Effective Linewidth in Maganese Substituted Single Crystal Barium Ferrite*, Journal of Applied Physics **73**, 4512 (1993).

[35] S. Emori, D. Yi, S. Crossley, J. J. Wisser, P. P. Balakrishnan, B. Khodadadi, P. Shafer, C. Klewe, A. T. N'Diaye, B. T. Urwin, K. Mahalingam, B. M. Howe, H. Y. Hwang, E. Arenholz, and Y. Suzuki, *Ultralow Damping in Nanometer-Thick Epitaxial Spinel Ferrite Thin Films*, Nano Lett. **18**, 4273 (2018).

[36] I. Harward, Y. Nie, D. Chen, J. Baptist, J. M. Shaw, E. Jakubisová Lišková, Š. Višňovský, P. Široký, M. Lesňák, J. Pištora, and Z. Celinski, *Physical Properties of Al Doped Ba Hexagonal Ferrite Thin Films*, Journal of Applied Physics **113**, 043903 (2013).

[37] H. Chang, P. Li, W. Zhang, T. Liu, A. Hoffmann, L. Deng, and M. Wu, *Nanometer-Thick Yttrium Iron Garnet Films With Extremely Low Damping*, IEEE Magnetics Letters **5**, 1 (2014).

[38] S. Crossley, A. Quindeau, A. G. Swartz, E. R. Rosenberg, L. Beran, C. O. Avci, Y. Hikita, C. A. Ross, and H. Y. Hwang, *Ferromagnetic Resonance of Perpendicularly Magnetized Tm3Fe5O12/Pt Heterostructures*, Appl. Phys. Lett. **115**, 172402 (2019).

[39] M. C. Onbasli, A. Kehlberger, D. H. Kim, G. Jakob, M. Kläui, A. V. Chumak, B. Hillebrands, and C. A. Ross, *Pulsed Laser Deposition of Epitaxial Yttrium Iron Garnet Films with Low Gilbert Damping and Bulk-like Magnetization*, APL Materials **2**, 106102 (2014).

[40] B. M. Howe, S. Emori, H.-M. Jeon, T. M. Oxholm, J. G. Jones, K. Mahalingam, Y. Zhuang, N. X. Sun, and G. J. Brown, *Pseudomorphic Yttrium Iron Garnet Thin Films With Low Damping and Inhomogeneous Linewidth Broadening*, IEEE Magnetics Letters **6**, 1 (2015).

[41] C. Hauser, T. Richter, N. Homonnay, C. Eisenschmidt, M. Qaid, H. Deniz, D. Hesse, M. Sawicki, S. G. Ebbinghaus, and G. Schmidt, *Yttrium Iron Garnet Thin Films with Very Low Damping Obtained by Recrystallization of Amorphous Material*, Scientific Reports **6**, 1 (2016).
[42] C. L. Jermain, H. Paik, S. V. Aradhya, R. A. Buhrman, D. G. Schlom, and D. C. Ralph, *Low-Damping Sub-10-Nm Thin Films of Lutetium Iron Garnet Grown by Molecular-Beam Epitaxy*, Appl. Phys. Lett. **109**, 192408 (2016).
[43] B. Bhoi, N. Venkataramani, R. P. R. C. Aiyar, S. Prasad, and M. Kostylev, *Effect of Annealing on the Structural and FMR Properties of Epitaxial YIG Thin Films Grown by RF Magnetron Sputtering*, IEEE Transactions on Magnetics **54**, 1 (2018).
[44] V. Kambersky and C. E. Patton, *Spin-Wave Relaxation and Phenomenological Damping in Ferromagnetic Resonance*, Phys. Rev. B **11**, 2668 (1975).
[45] V. Kambersky, B. Heinrich, and D. Fraitova, *INFLUENCE OF CONDUCTION ELECTRONS ON LINEWIDTHOF FMR IN METALS*, PHYSICS LETTERS **23**, 26 (1966).
[46] I. W. Haygood, M. R. Pufall, E. R. J. Edwards, J. M. Shaw, and W. H. Rippard, *Strong Coupling of Fe-Co Alloy with Ultralow Damping to Superconducting Co-Planar Waveguide Resonators*, ArXiv:2102.01129 [Cond-Mat] (2021).
[47] S. Mangin, D. Ravelosona, J. A. Katine, M. J. Carey, B. D. Terris, and E. E. Fullerton, *Current-Induced Magnetization Reversal in Nanopillars with Perpendicular Anisotropy*, Nat. Mater. **5**, 210 (2006).
[48] S. Trudel, O. Gaier, J. Hamrle, and B. Hillebrands, *Magnetic Anisotropy, Exchange and Damping in Cobalt-Based Full-Heusler Compounds: An Experimental Review*, J. Phys. D: Appl. Phys. **43**, 193001 (2010).
[49] S. Andrieu, A. Neggache, T. Hauet, T. Devolder, A. Hallal, M. Chshiev, A. M. Bataille, P. Le Fèvre, and F. Bertran, *Direct Evidence for Minority Spin Gap in the $\mathrm{C}{\mathrm{o}}_{2}\mathrm{MnSi}$ Heusler Compound*, Phys. Rev. B **93**, 094417 (2016).
[50] T. Kubota, S. Tsunegi, M. Oogane, S. Mizukami, T. Miyazaki, H. Naganuma, and Y. Ando, *Half-Metallicity and Gilbert Damping Constant in Co2FexMn1−xSi Heusler Alloys Depending on the Film Composition*, Applied Physics Letters **94**, 122504 (2009).
[51] C. Sterwerf, S. Paul, B. Khodadadi, M. Meinert, J.-M. Schmalhorst, M. Buchmeier, C. K. A. Mewes, T. Mewes, and G. Reiss, *Low Gilbert Damping in Co2FeSi and Fe2CoSi Films*, Journal of Applied Physics **120**, 083904 (2016).
[52] S. Mankovsky, D. Ködderitzsch, G. Woltersdorf, and H. Ebert, *First-Principles Calculation of the Gilbert Damping Parameter via the Linear Response Formalism with Application to Magnetic Transition Metals and Alloys*, Phys. Rev. B **87**, 014430 (2013).
[53] C. Scheck, L. Cheng, I. Barsukov, Z. Frait, and W. E. Bailey, *Low Relaxation Rate in Epitaxial Vanadium-Doped Ultrathin Iron Films*, Phys. Rev. Lett. **98**, 117601 (2007).
[54] T. Devolder, T. Tahmasebi, S. Eimer, T. Hauet, and S. Andrieu, *Compositional Dependence of the Magnetic Properties of Epitaxial FeV/MgO Thin Films*, Appl. Phys. Lett. **103**, 242410 (2013).
[55] M. Bersweiler, K. Watanabe, H. Sato, F. Matsukura, and H. Ohno, *Magnetic Properties of FeV/MgO-Based Structures*, Appl. Phys. Express **10**, 083001 (2017).
[56] J.-M. L. Beaujour, A. D. Kent, D. W. Abraham, and J. Z. Sun, *Ferromagnetic Resonance Study of Polycrystalline Fe1−xVx Alloy Thin Films*, Journal of Applied Physics **103**, 07B519 (2008).
[57] D. A. Smith, A. Rai, Y. Lim, T. Q. Hartnett, A. Sapkota, A. Srivastava, C. Mewes, Z. Jiang, M. Clavel, M. K. Hudait, D. D. Viehland, J. J. Heremans, P. V. Balachandran, T. Mewes, and S. Emori, *Magnetic Damping in Epitaxial Iron Alloyed with Vanadium and Aluminum*, Phys. Rev. Applied **14**, 034042 (2020).
[58] K. Gilmore, M. D. Stiles, J. Seib, D. Steiauf, and M. Fähnle, *Anisotropic Damping of the Magnetization Dynamics in Ni, Co, and Fe*, Phys. Rev. B **81**, 174414 (2010).

[59] E. R. J. Edwards, H. T. Nembach, and J. M. Shaw, *${\mathrm{Co}}_{25}{\mathrm{Fe}}_{75}$ Thin Films with Ultralow Total Damping of Ferromagnetic Resonance*, Phys. Rev. Applied **11**, 054036 (2019).
[60] H. T. Nembach, T. J. Silva, J. M. Shaw, M. L. Schneider, M. J. Carey, S. Maat, and J. R. Childress, *Perpendicular Ferromagnetic Resonance Measurements of Damping and Lande#x0301g- Factor in Sputtered (Co2Mn)1-XGex Thin Films*, Phys. Rev. B **84**, 054424 (2011).
[61] H. Ebert, D. Ködderitzsch, and J. Minár, *Calculating Condensed Matter Properties Using the KKR-Green's Function Method—Recent Developments and Applications*, Rep. Prog. Phys. **74**, 096501 (2011).
[62] P. Soven, *Coherent-Potential Model of Substitutional Disordered Alloys*, Phys. Rev. **156**, 809 (1967).
[63] G. M. Stocks, W. M. Temmerman, and B. L. Gyorffy, *Complete Solution of the Korringa-Kohn-Rostoker Coherent-Potential-Approximation Equations: Cu-Ni Alloys*, Phys. Rev. Lett. **41**, 339 (1978).
[64] J. P. Perdew, K. Burke, and M. Ernzerhof, *Generalized Gradient Approximation Made Simple*, Phys. Rev. Lett. **77**, 3865 (1996).
[65] H. Ebert, A. Vernes, and J. Banhart, *Relativistic Bandstructure of Disordered Magnetic Alloys*, Solid State Communications **104**, 243 (1997).
[66] H. Ebert, S. Mankovsky, K. Chadova, S. Polesya, J. Minár, and D. Ködderitzsch, *Calculating Linear-Response Functions for Finite Temperatures on the Basis of the Alloy Analogy Model*, Phys. Rev. B **91**, 165132 (2015).
[67] W. H. Butler, *Theory of Electronic Transport in Random Alloys: Korringa-Kohn-Rostoker Coherent-Potential Approximation*, Phys. Rev. B **31**, 3260 (1985).
[68] P. Villars and K. Cenzual, *Pearson's Crystal Data - Crystal Structure Database for Inorganic Compounds*.
[69] W. P. Davey, *Precision Measurements of the Lattice Constants of Twelve Common Metals*, Phys. Rev. **25**, 753 (1925).
[70] E. I. Gladyshevskii, *Iron-Silicon-Vanadium Ternary Alloy Phase Diagram*, Russ. Metall. **2**, 63 (1965).
[71] K. H. J. Buschow, P. G. van Engen, and R. Jongebreur, *Magneto-Optical Properties of Metallic Ferromagnetic Materials*, Journal of Magnetism and Magnetic Materials **38**, 1 (1983).
[72] H. Martens and P. Duwez, *Fe-V Something*, Trans. ASM **44**, 484 (1952).
[73] W. Zarek, M. Tuszyński, and E. S. Popiel, *Magnetic Properties of Fe2.6V1.4−xAlx Alloys*, Journal of Magnetism and Magnetic Materials **104–107**, 2067 (1992).
[74] A. M. van der Kraan, D. B. de Mooij, and K. H. J. Buschow, *Magnetic Properties and 57Fe Mössbauer Effect in V1–XFex Alloys*, Physica Status Solidi (a) **88**, 231 (1985).
[75] J.-I. Seki, M. Hagiwara, and T. Suzuki, *Metastable Order-Disorder Transition and Sigma Phase Formation in Fe-V Binary Alloys*, J Mater Sci **14**, 2404 (1979).
[76] C. Y. Ho, R. W. Powell, and P. E. Liley, *Thermal Conductivity of the Elements: A Comprehensive Review*, J. Phys. Chem. Ref. Data, Suppl., v. 3, No. 1, Pp. 1-796 (1974).
[77] M. S. Osofsky, L. Cheng, W. E. Bailey, K. Bussmann, and D. Parker, *Measurement of the Transport Spin Polarization of FeV Using Point-Contact Andreev Reflection*, Appl. Phys. Lett. **102**, 212412 (2013).
[78] J. M. Shaw, H. T. Nembach, T. J. Silva, and C. T. Boone, *Precise Determination of the Spectroscopic G-Factor by Use of Broadband Ferromagnetic Resonance Spectroscopya)*, Journal of Applied Physics **114**, 243906 (2013).
[79] M. A. W. Schoen, J. Lucassen, H. T. Nembach, T. J. Silva, B. Koopmans, C. H. Back, and J. M. Shaw, *Magnetic Properties of Ultrathin $3d$ Transition-Metal Binary Alloys. I. Spin and Orbital Moments, Anisotropy, and Confirmation of Slater-Pauling Behavior*, Phys. Rev. B **95**, 134410 (2017).

[80] G. Woltersdorf, M. Buess, B. Heinrich, and C. H. Back, *Time Resolved Magnetization Dynamics of Ultrathin Fe(001) Films: Spin-Pumping and Two-Magnon Scattering*, Phys. Rev. Lett. **95**, 037401/1 (2005).
[81] C. T. Boone, H. T. Nembach, J. M. Shaw, and T. J. Silva, *Spin Transport Parameters in Metallic Multilayers Determined by Ferromagnetic Resonance Measurements of Spin-Pumping*, Journal of Applied Physics **113**, 153906 (2013).
[82] B. D. Cullity, S. R. Stock, and S. R. Stock, *Elements of X-Ray Diffraction* (Prentice Hall, 2001).
[83] D. Thonig, Y. Kvashnin, O. Eriksson, and M. Pereiro, *Nonlocal Gilbert Damping Tensor within the Torque-Torque Correlation Model*, Phys. Rev. Materials **2**, 013801 (2018).
[84] O. Šipr, S. Mankovsky, and H. Ebert, *Spin Wave Stiffness and Exchange Stiffness of Doped Permalloy via Ab Initio Calculations*, Phys. Rev. B **100**, 024435 (2019).
[85] J. M. Shaw, H. T. Nembach, and T. J. Silva, *Roughness Induced Magnetic Inhomogeneity in Co/Ni Multilayers: Ferromagnetic Resonance and Switching Properties in Nanostructures*, J. Appl. Phys. **108**, 093922 (2010).
[86] M. A. W. Schoen, J. Lucassen, H. T. Nembach, B. Koopmans, T. J. Silva, C. H. Back, and J. M. Shaw, *Magnetic Properties in Ultrathin $3d$ Transition-Metal Binary Alloys. II. Experimental Verification of Quantitative Theories of Damping and Spin Pumping*, Phys. Rev. B **95**, 134411 (2017).
[87] S. U. Jen and G. Y. Chen, *Magnetostriction of Fe-Rich Fe–Co and Fe–V Alloys*, Journal of Magnetism and Magnetic Materials **204**, 165 (1999).
[88] S. U. Jen, T. L. Tsai, and C. C. Liu, *Magnetic Properties of Fe-Rich Fe–V Alloy Films*, Journal of Applied Physics **106**, 013901 (2009).
[89] S. Ostanin, J. B. Staunton, S. S. A. Razee, C. Demangeat, B. Ginatempo, and E. Bruno, *Ab Initio Search for a High Permeability Material Based on Bcc Iron*, Phys. Rev. B **69**, 064425 (2004).